Hybrid SONIC: joint feedforward-feedback narrowband interference canceller

Maciej Niedźwiecki[1], Michał Meller[1]

[1] *Faculty of Electronics, Telecommunications and Computer Science, Department of Automatic Control, Gdańsk University of Technology, ul. Narutowicza 11/12, Gdańsk, Poland, Tel: +48 58 3472519; fax: +48 58 3415821.*

SUMMARY

SONIC (Self-Optimizing Narrowband Interference Canceller) is an acronym of a recently proposed active noise control algorithm with interesting adaptivity and robustness properties. SONIC is a purely-feedback controller, capable of rejecting nonstationary sinusoidal disturbances (with time-varying amplitude and/or frequency) in the presence of plant (secondary path) uncertainty. We show that although SONIC can work reliably without access to a reference signal, even when the frequency of the disturbance is unknown and possibly time-varying, the algorithm can take advantage of such additional source information. Unlike classical hybrid solutions, the reference signal is used only to extract information about the instantaneous frequency of the disturbance. The advance-time advantage, available due to the fact that the acoustic delay in the system is larger than the electrical delay, allows one to incorporate in the control loop a smoothed, and hence more accurate, frequency estimate. This increases the attenuation efficiency of SONIC and widens its operating range - the modified algorithm can be safely used in the presence of rapid frequency changes. Copyright © 0000 John Wiley & Sons, Ltd.

Received . . .

KEY WORDS: active noise control, time-varying processes, adaptive signal processing

1. INTRODUCTION

Adaptive noise cancellers (ANCs) are traditionally divided into feedforward, feedback, and hybrid systems. A feedforward system relies on successive measurements of the so-called reference signal $r(t)$ – a signal strongly correlated with the disturbance, measured by a sensor (microphone, accelerometer) placed close to the source of unwanted sound (we will focus here on acoustic applications). Since the acoustic delay τ_{ac}, i.e., delay with which the sound wave emitted by the source of disturbance reaches the point at which it is supposed to be canceled, is considerably longer than the electrical delay τ_{el} with which reference measurements are transmitted to the control unit, the controller has the advantage of knowing the disturbance (or, more precisely, of knowing the signal correlated with the disturbance) before it reaches the cancellation point – see Fig. 1(a).

(a) Feedforward ANC

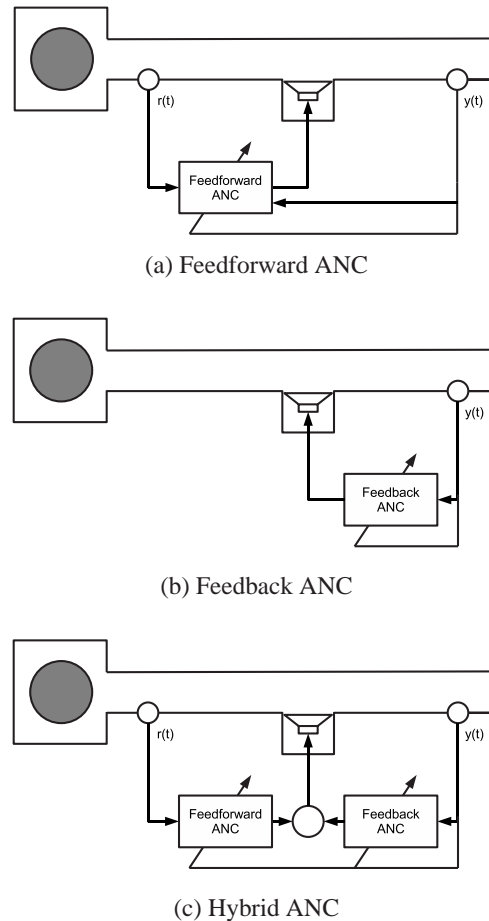

(b) Feedback ANC

(c) Hybrid ANC

Figure 1. Typical configurations of an ANC system for cancellation of noise in an acoustic duct.

The controller itself is an adaptive filter that transforms the reference signal into an "antisound" emitted by the canceling loudspeaker to achieve destructive interference. The FXLMS (filtered-X least mean squares) algorithm [1], [2] is perhaps the one most frequently used for this purpose in acoustic applications. In the control literature, the task described above is known as the disturbance rejection problem. Its elegant solutions, based on the so-called "internal model principle", are now available for a very general class of systems (continuous-time, nonlinear, and uncertain) – for recent advances see e.g. [3], [4] and references therein.

For truly wideband (i.e., "unpredictable") disturbances, such as white noise, feedforward compensation is the only *plausible* solution. It works as long as the following causality condition is fulfilled

$$\tau_{\text{ac}} \geq \tau_{\text{el}} + \tau_{\text{pr}} \tag{1}$$

where τ_{pr} denotes the processing delay introduced by the controller.

When the disturbance is narrowband, i.e., predictable from its past, the causality constraint does not apply. In such a case, cancellation can be performed using a feedback controller [1]–[4], i.e., a system that relies entirely on measurements of the error signal $y(t)$ – see Fig. 1(b). An attractive feedback ANC algorithm, based on a new control paradigm, was proposed recently in [5], [6]. This algorithm, called SONIC (Self-Optimizing Narrowband Interference Canceller), has several

advantages over classical (e.g., FXLMS-based) solutions – due to its self-optimization property, it can cope favorably with both disturbance and plant nonstationarity, avoids nonidentifiability problems that often arise when estimation is carried out in a closed loop, and is computationally simple.

Finally, in the so-called hybrid ANC systems, the cancelling signal is worked out based on both reference measurements $r(t)$ and error measurements $y(t)$. The idea of a hybrid approach can be traced back to the papers of Swanson [7] and Zangi [8] (see also [2] and [9]). Some more recent studies that consider hybrid control for acoustic noise cancellation include [10]–[13].

Hybrid systems are usually made up of two components: the feedforward ANC, which attenuates primary noise that is correlated with the reference signal, and the feedback ANC, which cancels the predictable components of the primary noise that are not observed by the reference sensor – see Fig. 1(c). Our design philosophy is different. Focused on cancellation of *nonstationary* sinusoidal disturbances, with time-varying amplitudes and frequencies, we redesign the SONIC algorithm so that it can take advantage of information provided by the reference sensor. Unlike most of the existing hybrid schemes, hybrid SONIC is *not* made up of two controllers – the reference signal is used only to extract information about the instantaneous frequency of the disturbance, rather than to form a reference-dependent control (compensation) signal. Therefore, it can be characterized as a feedback ANC with an external (feedforward) frequency adjustment mechanism. Since the reference signal is usually a more reliable source of information about the instantaneous frequency of the disturbance than the error signal (which is minimized by the controller), hybrid SONIC has better tracking and robustness properties than its original, purely feedback version. It also performs better than the classical, general-purpose hybrid schemes, such as the one proposed by Zangi [8].

2. SONIC [5], [6] – AN OVERVIEW

A block diagram of the SONIC canceller is shown in Fig. 2. The algorithm was derived assuming that the error signal $y(t)$ (output of the ANC system) can be written in the form

$$y(t) = K(q^{-1})u(t-1) + d(t) + v(t) \qquad (2)$$

where $t = \ldots, -1, 0, 1, \ldots$ denotes normalized (dimensionless) discrete time, $K(q^{-1})$ denotes the unknown transfer function of the secondary path (q^{-1} is the backward shift operator), $u(t)$ denotes the input signal generated by the controller, $d(t)$ denotes a nonstationary narrowband disturbance, and $v(t)$ is wideband measurement noise. To make the analysis simpler, all signals specified above are assumed to be complex-valued.

Furthermore, it was assumed that the nonstationary disturbance is governed by

$$d(t) = \beta(t)e^{j\phi(t)}, \ \beta(t) = a(t)e^{j\varphi_0}, \ \phi(t) = \sum_{i=1}^{t-1} \omega(i) \qquad (3)$$

where $\omega(t)$ denotes the slowly-varying instantaneous frequency and $a(t)$ is a slowly-varying (real-valued) amplitude. Note that $\beta(t)$ incorporates the initial phase φ_0 of the cisoid.
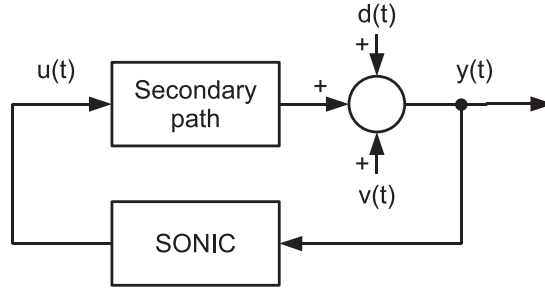
Figure 2. Block diagram of a SONIC-based ANC system

SONIC [5], [6] can be summarized as follows:

$$self\ optimization:$$

$$z(t) = e^{j\widehat{\omega}(t)} \left[(1 - c_\mu)z(t-1) - \frac{c_\mu}{\widehat{\mu}(t-1)}y(t-1) \right]$$

$$p(t) = \rho p(t-1) + |z(t)|^2$$

$$\widehat{\mu}(t) = \widehat{\mu}(t-1) - \frac{y(t)z^*(t)}{p(t)} \tag{4}$$

$$predictive\ control:$$

$$\widehat{d}(t+1|t) = e^{j\widehat{\omega}(t)}[\widehat{d}(t|t-1) + \widehat{\mu}(t)y(t)]$$

$$u(t) = -\frac{\widehat{d}(t+1|t)}{k_{\mathrm{n}}[\widehat{\omega}(t)]} \tag{5}$$

$$frequency\ estimation:$$

$$\widehat{\omega}(t+1) = \widehat{\omega}(t) + \gamma \operatorname{Im}\left[\frac{\widehat{\mu}(t)y(t)}{\widehat{d}(t|t-1)} \right]. \tag{6}$$

where c_μ, ρ, k_{n} and γ are user-dependent "knobs" described below.

The control part of the algorithm works out the one-step-ahead prediction of the disturbance, based on the instantaneous frequency estimates $\widehat{\omega}(t)$ provided by a simple gradient search algorithm (γ, $0 < \gamma < 1$, denotes a small adaptation gain). The quantity $k_{\mathrm{n}}[\widehat{\omega}(t)] = K_{\mathrm{n}}(e^{j\widehat{\omega}(t)})$, which is involved in computation of the control signal $u(t)$, denotes the "nominal" (assumed) gain of the secondary path at the frequency $\widehat{\omega}(t)$, usually different from the true gain $K(e^{j\widehat{\omega}(t)})$. When no prior knowledge of $K(q^{-1})$ is available, one can fix the nominal gain by setting, for example, $K_{\mathrm{n}}(q^{-1}) \equiv 1$.

Finally, $\widehat{\mu}(t)$ denotes a complex-valued adaptation gain, adjusted so as to minimize the local (exponentially weighted) error criterion

$$V(t) = \sum_{i=0}^{\infty} \rho^i |y(t-i)|^2$$

where $\rho \cong 1$ $(0 < \rho < 1)$ denotes the forgetting constant. Due to the fact that the gain $\widehat{\mu}(t)$ is complex-valued, the self-optimization part of the algorithm can simultaneously achieve two goals: compensation of modeling errors and adjustment of the controller bandwidth to the rate of disturbance nonstationarity [5]. The quantity $z(t)$, incorporated in the optimization process, can be interpreted as the output sensitivity derivative

$$z(t) = \frac{\partial y[t, \widehat{\mu}(t-1)]}{\partial \mu}$$

and $c_\mu > 0$ denotes a small constant.

The multifrequency version of SONIC was presented in [14].

Remark: The frequency-update recursion (6) differs from that proposed in [6]:

$$\widehat{\omega}(t+1) = (1-\gamma)\widehat{\omega}(t) + \gamma \operatorname{Arg}\left[\frac{\widehat{d}(t+1|t)}{\widehat{d}(t|t-1)}\right] \tag{7}$$

where $\operatorname{Arg}[x] \in (-\pi, \pi]$ denotes a principal argument of a complex number x. While for $\mu \to 0$ and $\gamma \to 0$, both algorithms have asymptotically the same statistical properties, (6) is computationally more attractive than (7), as it does not involve trigonometric operations (inverse tangent), and is immune to the phenomenon known as phase wrapping.

3. HYBRID SONIC

An obvious advantage of SONIC, typical of all feedback ANC systems, is due to the fact that it does not require deployment of a reference sensor. Such a sensor may be expensive and/or difficult to mount. Additionally, it may introduce acoustic feedback, which deteriorates performance of the ANC system. However, this advantage comes at a price: without access to a reference signal, SONIC needs to learn the properties of the disturbance, such as its instantaneous frequency $\omega(t)$, by observing the error signal $y(t)$, i.e., the very signal it is trying to cancel. Such an internal "conflict of interests" (things that are good for identification are bad for control and *vice versa*) is an inherent limitation of many adaptive control systems. Under nonstationary conditions, this may result in episodes of turbulent, or even bursting, behavior, not acceptable from a practical viewpoint.

The controller proposed in this paper is based on the observation that it may be worthwhile to replace the feedback estimate $\widehat{\omega}(t)$ of the instantaneous frequency with an appropriately modified (smoothed or simply delayed) feedforward estimate $\widehat{\omega}_0(t)$ obtained by means of processing a reference signal

$$r(t) = d_0(t) + v_0(t) \tag{8}$$

where $d_0(t)$ denotes the narrowband signal emitted by the disturbance source, and $v_0(t)$ denotes measurement noise, independent of $v(t)$, picked up by the reference sensor. Such a hybrid solution, depicted in Fig. 3, has two advantages over the purely feedback design:
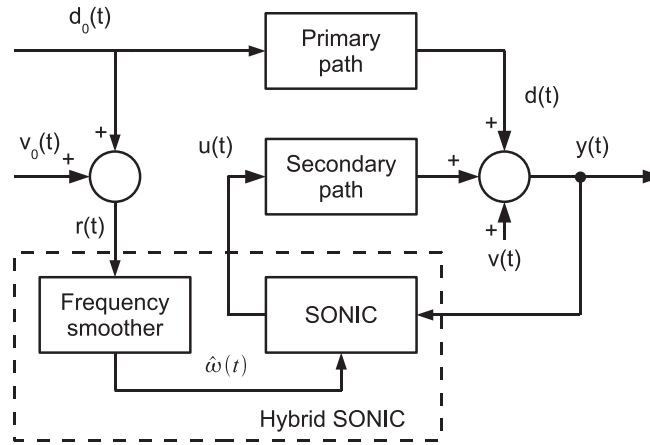
Figure 3. Block diagram of a hybrid SONIC-based ANC system

1. The reference signal is a non-vanishing source of information about the instantaneous frequency of the disturbance. Additionally, even if the ANC system is switched off, the signal-to-noise ratio is usually much higher at the reference point than at the cancellation point.

2. Since the reference signal is measured ahead of time, estimation of the instantaneous frequency of $d(t)$ can be based not only on the past, but also on a certain number of "future" (relative to the local time of the controller) samples of the disturbance. Such noncausal estimates, which incorporate smoothing, are more accurate than their causal counterparts.

The hybrid SONIC algorithm consists of two loops described below.

3.1. Feedforward Loop – Frequency Estimation

3.1.1. Frequency tracking Estimation of the instantaneous frequency $\omega_0(t)$ of the nonstationary cisoid $d_0(t)$ can be carried out using the adaptive notch filtering (ANF) algorithm given below (a modified version of the algorithm presented in [15]):

$$\varepsilon(t) = r(t) - \widehat{d}_0(t|t-1)$$
$$\widehat{d}_0(t+1|t) = e^{j\widehat{\omega}_0(t)}[\widehat{d}_0(t|t-1) + \mu_0\varepsilon(t)]$$
$$\widehat{\omega}_0(t+1) = \widehat{\omega}_0(t) + \gamma_0\mu_0 \, \mathrm{Im}\left[\frac{\varepsilon(t)}{\widehat{d}_0(t|t-1)}\right] \tag{9}$$

where μ_0 $(0 < \mu_0 \ll 1)$ and γ_0 $(0 < \gamma_0 \ll 1)$ are small step sizes determining the rate of amplitude adaptation and frequency adaptation, respectively. Although this algorithm resembles the analogous one incorporated in (6), there is one important difference – the step size μ_0 used in (9) is fixed (time-invariant) and real-valued.

It should be noted that, in spite of its simplicity, the algorithm (9) has very good statistical properties: when the instantaneous frequency drifts according to the random-walk model, the optimally-tuned tracker is (under Gaussian assumptions) statistically efficient, i.e., it reaches a Cramér-Rao-type lower frequency tracking bound [15].

The frequency tracking properties of the ANF algorithm (9) can be analyzed using the approximating linear filter (ALF) technique – the stochastic linearization approach proposed in [16]. Suppose that $d_0(t)$ is a constant-modulus cisoid governed by

$$d_0(t+1) = e^{j\omega_0(t)}d_0(t), \ \ |d_0(t)|^2 = a_0^2, \ \forall t \tag{10}$$

and that $v_0(t)$ is zero-mean circular white noise with variance $\sigma_{v_0}^2$. Using the ALF technique, one can show that (see Appendix)

$$\widehat{\omega}_0(t) \cong H_1(q^{-1})e(t) + H_2(q^{-1})\omega_0(t) \tag{11}$$

where

$$e(t) = \mathrm{Im}[v_0(t)d_0^*(t)]/a_0^2$$

denotes zero-mean real-valued white noise with variance $\sigma_e^2 = \sigma_{v_0}^2/(2a_0^2)$ and

$$H_1(q^{-1}) = \frac{\gamma_0\mu_0(1-q^{-1})q^{-1}}{D(q^{-1})} \ , \ \ H_2(q^{-1}) = \frac{\gamma_0\mu_0 q^{-2}}{D(q^{-1})}$$

$$D(q^{-1}) = 1 - (2 - \mu_0)q^{-1} + (1 - \mu_0 + \gamma_0\mu_0)q^{-2}.$$

Remark: Note that while the transfer function $H_1(q^{-1})$ coincides with that derived in [6] for the original SONIC algorithm, the transfer function $H_2(q^{-1})$, which is of primary interest here, has a different form – see [4, eq. (12)].

3.1.2. Frequency debiasing Since the reference signal is known ahead of time, the control unit can use smoothed estimates of the instantaneous frequency $\omega(t)$. Denote by

$$\bar{\omega}_0(t) = \mathrm{E}[\widehat{\omega}_0(t)|\omega_0(s), s \leq t] = H_2(q^{-1})\omega_0(t) \tag{12}$$

the mean path of frequency estimates for a particular frequency trajectory. Since $H_2(q^{-1})$ is a lowpass filter with unity static gain $H_2(1) = 1$, for a slowly-varying instantaneous frequency it holds that

$$\mathrm{E}[\widehat{\omega}_0(t)|\omega_0(s), s \leq t] \cong \omega_0(t - \tau_{\mathrm{est}}) \tag{13}$$

where $\tau_{\mathrm{est}} = \mathrm{int}[t_\omega]$ and

$$t_\omega = -\lim_{\xi \to 0} \frac{d\left\{\arg[H_2(e^{-j\xi})]\right\}}{d\xi} = \frac{1}{\gamma_0} \tag{14}$$

denotes a nominal (low-frequency) delay introduced by the filter $H_2(q^{-1})$. According to (13), $\widehat{\omega}_0(t)$ can be viewed as an estimate of $\omega_0(t - \tau_{\mathrm{est}})$. This can be symbolically written in the form

$$\widehat{\omega}_0(t) \longleftrightarrow \omega_0(t - \tau_{\mathrm{est}}). \tag{15}$$

Hence, delaying the estimate $\widehat{\omega}_0(\cdot)$ by τ_{est} samples is the simplest way of obtaining smoothed estimates of the instantaneous frequency $\omega_0(\cdot)$.
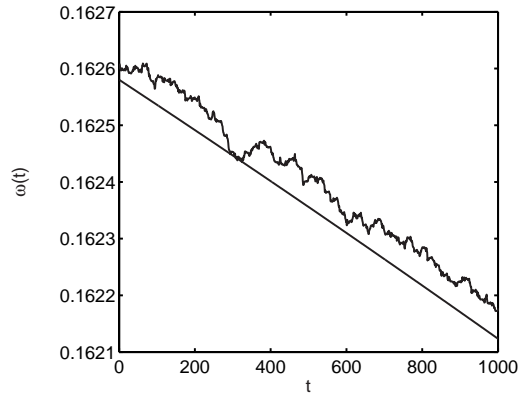
Figure 4. A fragment of a true-frequency trajectory (smooth line) and its estimated version (ragged line) obtained in the case where the estimation delay is equal to 100 samples.

We note that τ_{est} is the optimal delay, i.e., the time shift that minimizes the bias component of the mean-squared frequency estimation error (its variance component is invariant with respect to time shifts). When the admissible delay is smaller than τ_{est}, bias reduction is less efficient, but still may be significant – more so for larger delay. It doesn't make sense, though, to increase delay beyond τ_{est}.

The estimation delay effect is illustrated in Fig. 4, showing the results of the instantaneous frequency tracking, obtained for the signal

$$d_0(t) = 0.05 \sin[\phi_0(t)], \quad \phi_0(t) = \phi_0(t-1) + \omega_0(t)$$

$$\omega_0(t) = 0.05\pi \left[1 + 0.05 \sin \frac{2\pi t}{T_0} \right]$$

contaminated with zero-mean white Gaussian noise with variance $\sigma_{v_0}^2 = 10^{-6}$ (SNR= 20 dB). The estimation was carried out using the ANF algorithm (9) with adaptation gains set to $\mu_0 = 0.02$ and $\gamma_0 = 0.01$ ($\tau_{\text{est}} = 100$). The period of nostationarity T_0 was set to 80000 (which corresponds to 10 s for 8-kHz sampling). As expected, the estimated frequency trajectory is delayed with respect to the true trajectory by approximately 100 samples.

Fig. 5 shows the dependence of the mean-squared value of the frequency estimation error

$$\Delta\omega(t) = \omega_0(t) - \widehat{\omega}_0(t - \tau)$$

on the delay τ for two SNRs (10 dB, 20 dB). For the higher SNR value, the benefits of using the smoothed (delayed) frequency estimates are quite evident. Exactly as predicted by theory, the estimation error decreases with τ, until τ reaches τ_{est}; then for $\tau > \tau_{\text{est}}$, it gradually increases.

Note that due to the acoustic delay introduced by the primary path, the instantaneous frequency of the disturbance $d(\cdot)$ observed at the cancellation point at instant t can be approximated by the instantaneous frequency of the disturbance $d_0(\cdot)$ observed at the reference point at the instant $t - \tau_0$,
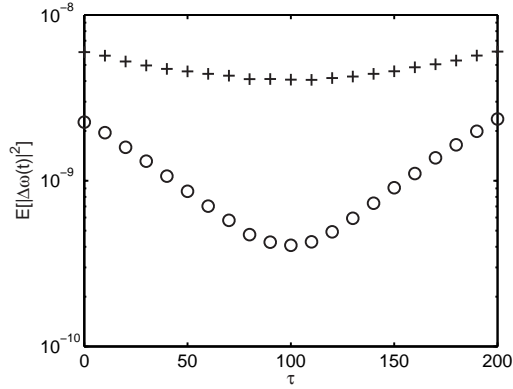
Figure 5. Dependence of mean-squared frequency estimation error on alignment delay τ for two SNR values: 10 dB $(+)$ and 20 dB $(\circ)$.

where $\tau_0 = \tau_{\mathrm{ac}} - \tau_{\mathrm{el}} - \tau_{\mathrm{pr}}$, or symbolically:

$$\omega(t) \longleftrightarrow \omega_0(t - \tau_0). \tag{16}$$

Of course, since the primary path is not a pure delay, this time-shifting property holds only approximately.

Combining (15) with (16), the (partially) debiased estimate of $\omega(t)$ can be obtained in the form

$$\widehat{\omega}(t) = \widehat{\omega}_0(t - \tau_{\mathrm{d}}). \tag{17}$$

where $\tau_{\mathrm{d}} = \max\{\tau_0 - \tau_{\mathrm{est}}, 0\}$.

3.2. Feedback loop – self-optimizing control

This part of the original SONIC algorithm, constituted by (4) and (5), remains unchanged, except that the feedback frequency estimates, given by (6), are replaced by the debiased estimates (17).

4. SIMULATION RESULTS

To check the potential benefits offered by the hybrid approach, two simulation experiments were performed. As documented in [5], [6], under nonstationary conditions, SONIC performs better than FXLMS-based solutions. For this reason, the proposed hybrid algorithm was compared only with the standard frequency-adaptive version of SONIC, given by (4)–(6), and with the classical hybrid solution proposed by Zangi [8].

Since all results presented in this paper apply to systems with inputs and outputs described by complex numbers, the generated real-valued signals $d_0(t)$, $d(t)$, $v_0(t)$, and $v(t)$ were converted to the complex format by adding zero imaginary parts. For cancellation purposes, we used $u_{\mathrm{R}}(t) = \mathrm{Re}[u(t)]$ – the real-part of the complex-valued signal $u(t)$ provided by SONIC. Similarly, the complex-valued error signal $\varepsilon(t)$ was replaced in (9) with $\varepsilon_{\mathrm{R}}(t) = \mathrm{Re}[r(t) - \widehat{d}_0(t|t-1)] =$

$r(t) - \text{Re}[\widehat{d}_0(t|t-1)]$. A more sophisticated approach to real-valued computations was described in [17].

The primary disturbance $d_0(t)$, with time-varying amplitude[†] and frequency (see Fig. 6), was generated by filtering the nonstationary sinusoidal signal

$$s(t) = 0.05 \sin[\phi(t)] , \ \ \phi(t) = \phi(t-1) + \omega(t)$$

by an impulse response $K_s(q^{-1})$ taken from a real acoustic source (established experimentally), giving

$$d_0(t) = K_s(q^{-1})s(t) \tag{18}$$

where the instantaneous angular frequency of $s(t)$ is governed by

$$\omega(t) = 0.05\pi \left[1 + 0.05 \sin \left(\frac{2\pi t}{T_0} + \psi_0 \right) \right]$$

where $T_0 \in [8000, 800000]$ and ψ_0 denotes a random variable with uniform distribution on the interval $[0, 2\pi)$, i.e., $\omega(t)$ varies sinusoidally around the nominal frequency $\omega_* = 0.05\pi$. Under 8-kHz sampling, this is equivalent to changes around $200\,\text{Hz}$ ($\pm 10\,\text{Hz}$) with the period ranging from $1\,\text{s}$ to $100\,\text{s}$.

During high-SNR-reference tests, the standard deviations of the primary and secondary white measurement noise were identical and equal to $\sigma_v = \sigma_{v_0} = 0.001$ – in the absence of disturbance cancellation, the corresponding SNR values ranged between $38\,\text{dB}$ and $47\,\text{dB}$ at the reference point, and between $33\,\text{dB}$ and $37\,\text{dB}$ at the cancellation point.

During low-SNR-reference tests, performed to check sensitivity of the control system to the "quality" of the reference signal, the standard deviation of the primary noise was increased to $\sigma_{v_0} = 0.0031$ (resulting in a 10-dB decrease of the input SNR level), while the intensity of the secondary noise remained unchanged.

All results reported below were obtained by joint time averaging (180000 time steps) and ensemble averaging (20 realizations of noise, the same in all experiments). To eliminate transient effects due to system initialization, the results obtained during the first 20000 time steps were discarded.

Experiment 1

In this experiment, three approaches were compared: the standard SONIC, the proposed hybrid version of SONIC with debiased frequency estimates, and a special variant of SONIC where information about the true instantaneous frequency of the disturbance, obtained by delaying the (known) instantaneous frequency of $s(t)$, was sent to the control unit. The latter configuration served as a reference, even though it is *not* the best case possible – since the disturbance signal is nonstationary, knowing its instantaneous frequency at the reference point is not equivalent to knowing its frequency at the cancellation point: the time-shifting property (16) is only approximately true. It was assumed that the feedback coupling between the reference sensor and

---

[†]Note that the signal $d_0(t)$ has time-varying amplitude even though the amplitude of $s(t)$ is constant. This is a typical effect observed when the filtered narrowband signal is nonstationary.
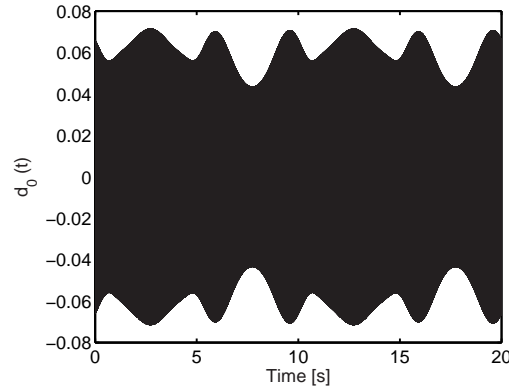
Figure 6. Example of primary disturbance $d_0(t)$ used in simulation experiments (generated for $T_0 = 80000$, which under 8-kHz sampling corresponds to a period of 10 s).

the canceling speaker can be neglected (which is appropriate for nonacoustic sensors, such as an accelerometer or tachometer).

The primary and secondary paths were simulated using finite-impulse-response models of a real acoustic duct. The corresponding impulse responses, shown in Fig. 7, were established under 8-kHz sampling. The primary and secondary delays were equal to 100 samples and 60 samples, respectively, i.e., the acoustic delay was roughly equal to $\tau_{ac} = 40$ samples.

The compared algorithms used identical settings in the self-optimization layer: $c_\mu = 0.0005$ and $\rho = 0.999$. Furthermore, to avoid erratic behavior during initial transients, all algorithms were modified by forcing additional constraints $1 < p(t) \le 100$ and $0.0005 < |\hat{\mu}(t)| \le 0.005$. In spite of the fact that the gain of the secondary path varies considerably in the vicinity of ω_*, the nominal gain was in all cases constant and equal to the true gain at the frequency ω_*: $k_n = K(e^{j\omega_*}) = 1.9 + j0.48$.

The frequency estimation step size of extended SONIC was set to $\gamma = 0.0025$. Although this value may seem small, it was found that using larger gains resulted in stability problems, caused by excessive transport delay in the feedback loop. On the other hand, the frequency estimation mechanism employed in the hybrid version of SONIC could enjoy the benefit of higher estimation gain: $\mu_0 = 0.02$, $\gamma_0 = 0.01$. Note that, under such settings, $\tau_{est} = 100$ and the optimal choice of smoothing delay in (17) is $\tau_d = 0$, i.e., the instantaneous frequency estimates, obtained by means of processing the reference signal, were employed immediately.

The performance of all algorithms was compared using cancellation error, defined as

$$c(t) = d(t) - K(q^{-1})u_R(t-1) .$$

The results, depicted in Fig. 8, show that considerable improvement can be obtained using the hybrid approach. Not only were the cancellation errors reduced by approximately one order of magnitude, but also the operating range of the system was widened – the modified algorithm can be safely used in the presence of 10 times faster frequency changes. Note that the improved algorithm even performs better than SONIC with full knowledge of disturbance frequency, and that the results almost did not change when the reference signal was contaminated with stronger noise. However, if the SNR is reduced by another 10 dB, the hybrid version of the canceller experiences occasional
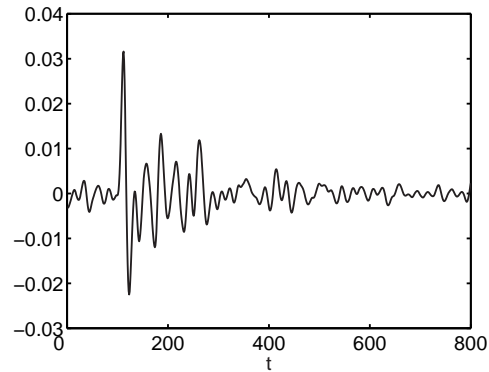
(a) Primary path
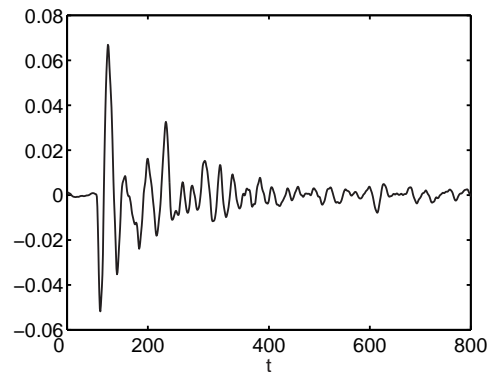
(b) Secondary path

Figure 7. Simulated impulse responses.

bursts of cancellation (not shown here) – the frequency estimator is unable to maintain proper tracking under such severe operating conditions.
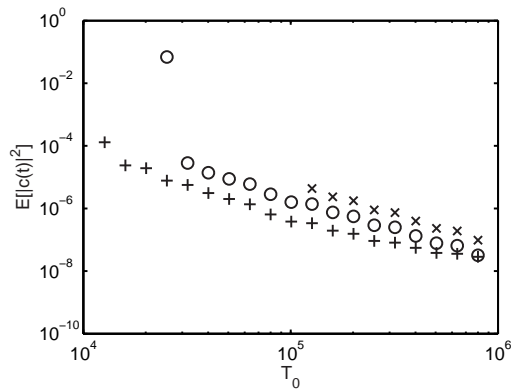
Experiment 2

The second experiment was designed to analyze the dependence of the mean-squared cancellation error on the relative delay τ_0 between primary and feedback paths. In order to check this, the length of the simulated acoustic duct was artificially increased/decreased by increasing/decreasing the primary delay, but without changing the shape of the corresponding impulse responses depicted in Fig. 7. Such a procedure guarantees that the observed performance changes can be attributed exclusively to the underlying changes in τ_0.

The results of this experiment, obtained under two SNR conditions, are shown in Fig. 9 for a fixed rate of disturbance nonstationarity ($T_0 = 320000$, which corresponds to 40 s under 8-kHz sampling). Note that the performance systematically improves with growing τ_0 until it reaches the saturation point at $\tau_0 = \tau_{\text{est}} = 100$.

The main source of performance improvement is due to the fact that the reference signal is a nonvanishing and hence a more reliable source of frequency information than the error signal. For $\tau_0 = 0$, i.e., when the smoothing action is absent (because of the lack of the advance-time advantage that could be used for this purpose), the mean-squared cancellation error of hybrid SONIC stays
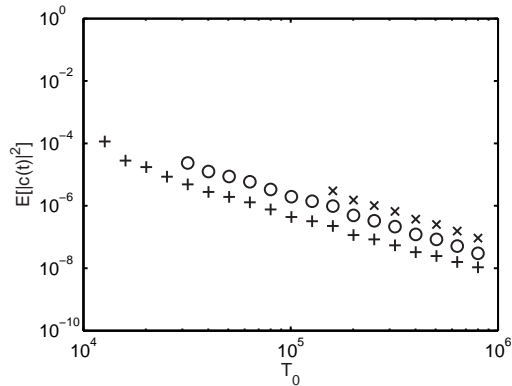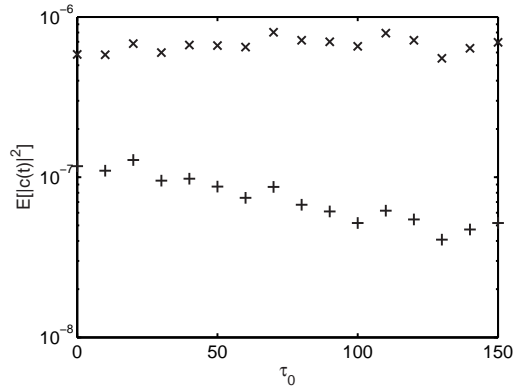
(a) High-SNR-reference conditions.

(b) Low-SNR-reference conditions.

Figure 8. Experiment 1: Comparison of the mean-squared cancellation error, plotted versus the time-varying-frequency period T_0, yielded by SONIC with feedback frequency tracking ($\times$), SONIC with full knowledge of the instantaneous frequency of the disturbance ($\circ$), and by hybrid SONIC with frequency debiasing ($+$).

7 dB below that yielded by the SONIC controller with feedback frequency tracking. Smoothing, which takes place when $\tau_0 > 0$, increases the attenuation of hybrid SONIC, but its effect is less pronounced, ranging from 6 dB under high-SNR-reference conditions to 3 dB under low-SNR-reference conditions (both values correspond to $\tau_0 = 100$, which is the largest smoothing rate possible in the case considered). This suggests that only marginal improvement can be expected when the simple frequency debiasing scheme, described in this paper, is replaced with the more sophisticated smoothing procedures proposed in [15] and [18]. Our other simulation experiments (not reported here) confirmed this conjecture.

Typical Output Signals

The results obtained for a typical simulation run ($T_0 = 160000$, $\tau_0 = 40$, $\sigma_v = \sigma_{v_0} = 0.001$) are shown in Fig. 10. Note the fluctuations of the output signal in Fig. 10(b) where the frequency is estimated in the feedback loop. Fig. 11, which is a close-up of Fig. 10(c), shows initialization transients yielded by hybrid SONIC. The attenuation efficiency, which in the time plots is partially masked by the measurement noise $v(t)$, is revealed by the average spectrogram plots shown in Fig. 12.

(a) High-SNR-reference conditions.
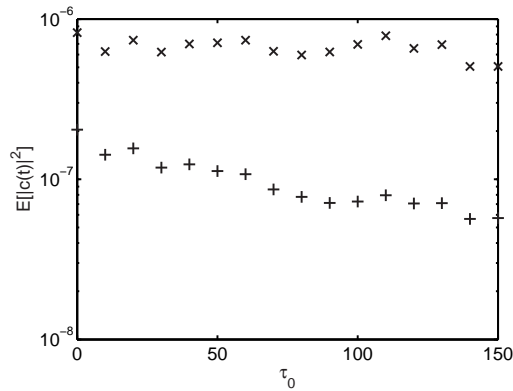
(b) Low-SNR-reference conditions.

Figure 9. Experiment 2: Dependence of the mean-squared cancellation error on the relative delay τ_0 (measured in samples) between primary and feedback paths, observed for SONIC with feedback frequency tracking ($\times$), and for hybrid SONIC with frequency debiasing ($+$).
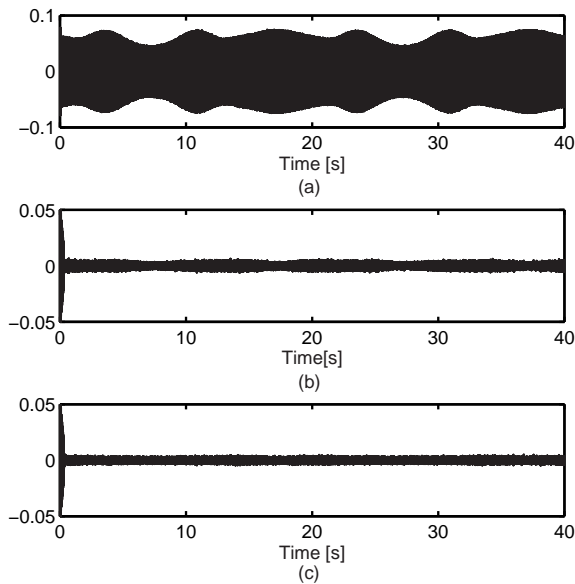

Figure 10. Time plots of the signals observed at the output of the simulated acoustic system (in all cases the same realization of measurement noise was used). (a) Without adaptive noise control. (b) With SONIC-based adaptive noise control. (c) With hybrid-SONIC-based adaptive noise control.
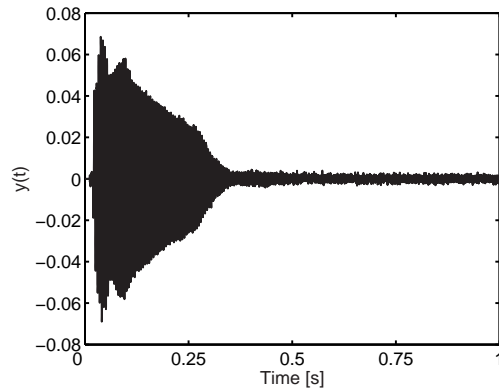
Figure 11. Initial convergence of the signal observed at the output of the simulated acoustic system governed by the hybrid SONIC controller.
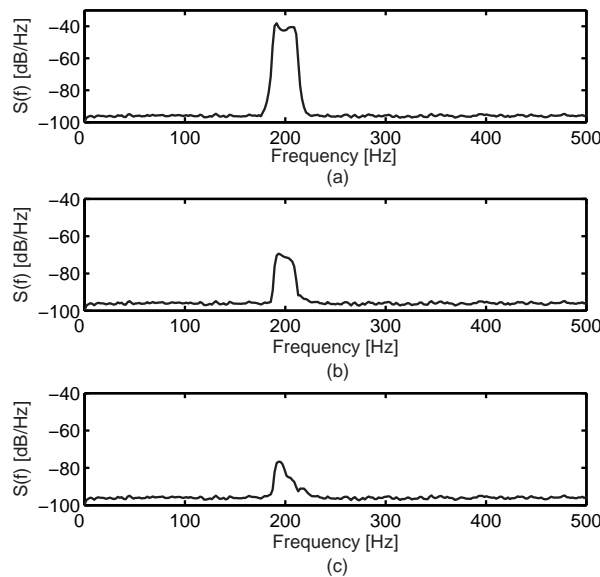

Figure 12. Average spectrograms of the signals observed at the output of the simulated acoustic system (in all cases the same realization of measurement noise was used). (a) Without adaptive noise control. (b) With SONIC-based adaptive noise control. (c) With hybrid-SONIC-based adaptive noise control.

Experiment 3

The aim of this experiment was to compare hybrid SONIC with the classical hybrid ANC – the Zangi's two-sensor algorithm [8]. In the scheme proposed by Zangi, which was chosen because of its relatively low computational complexity and good performance compared to the classical FXLMS algorithm, the cancelling signal is a linear combination of L past values of the reference signal (the feedforward component of the control signal) and L past values of the cancelled disturbance (the feedback component of the control signal)

$$u(t) = \sum_{i=0}^{L-1} a_i(t)r(t-i) + \sum_{i=0}^{L-1} b_i(t)d(t-i) = \mathbf{x}^{\mathrm{T}}(t)\mathbf{w}(t) \tag{19}$$

where $\mathbf{w}(t) = [a_0(t), \ldots, a_{L-1}(t), b_0(t), \ldots, b_{L-1}(t)]^{\mathrm{T}}$ and $\mathbf{x}(t) = [r(t), \ldots, r(t-L+1), d(t), \ldots, d(t-L+1)]^{\mathrm{T}}$, i.e., it is the output of a two-input FIR filter whose inputs are $r(t)$ and $d(t)$. Although the signal $d(t)$ is not directly measured, it can be easily estimated by subtracting the known cancelling signal from $y(t)$:

$$\widehat{d}(t) = y(t) - \widehat{K}(q^{-1})u(t-1) \tag{20}$$

where

$$\widehat{K}(q^{-1}) = \sum_{i=0}^{M-1} \widehat{k}_i q^{-i}$$

denotes the FIR model of the secondary path, obtained experimentally in the off-line mode.

The $2L \times 1$ vector of weighting coefficients $\mathbf{w}(t)$ is continuously adjusted by the standard FXLMS adaptation algorithm, driven by the error signal $y(t)$:

$$\mathbf{w}(t) = \mathbf{w}(t-1) + \eta \mathbf{x}'(t)y(t) \tag{21}$$

where $\eta > 0$ denotes a small adaptation step size, and

$$\mathbf{x}'(t) = \widehat{K}(q^{-1})\mathbf{x}(t)$$

denotes the filtered regression vector ("filtered-X").

Fig. 13 compares the cancelling efficiency of the two-sensor algorithm and the hybrid SONIC algorithm., for two signal-to-noise ratios (10 dB, 20 dB) and different values of the "period of nonstationarity" T_0. To be as fair as possible to the two-sensor algorithm, its design parameters were pre-optimized (the best results were obtained for $L = 40$ and $\eta = 0.02$), and secondary path modeling errors were not incorporated, i.e., it was assumed that $\widehat{K}(q^{-1}) = K(q^{-1})$. Note that even under such ideal conditions, hybrid SONIC outperforms the two-sensor algorithm for $T_0 \geq 10^5$ – see Fig. 13(a). When the parameters of the two-sensor algorithm are chosen less carefully ($L = 24$, $\eta = 0.01$), the performance gains reach 10 dB, and they extend over the entire range of T_0's – see Fig. 13(b).

In contrast to the two-sensor algorithm, hybrid SONIC does not need precise information (if any) about the transfer function of the secondary path – it automatically adapts to unknown and/or time-varying operating conditions, such as secondary path characteristics, signal-to-noise ratio, and the rate of frequency variation - see [5], [6] for more details. This explains its better cancellation properties.

For real-valued systems, the computational burden associated with the hybrid SONIC algorithm is equal to 32 real multiply/add operations, 3 real division operations, and 2 sine/cosine operations per time update. The analogous count for the two-sensor algorithm gives $3M + 4L + 1$ multiply/add operations per time update. Note that in our simulations, corresponding to 8-kHz sampling, M was equal to 800 and L was greater than 20, making the two-sensor algorithm computationally much more demanding than the hybrid SONIC algorithm. This observation remains true even if the sampling rate is reduced to 1 kHz, allowing one to use $M = 100$. We note, however, that the computational advantage of hybrid SONIC diminishes with increasing number of sinusoidal components m, as it grows linearly with m.
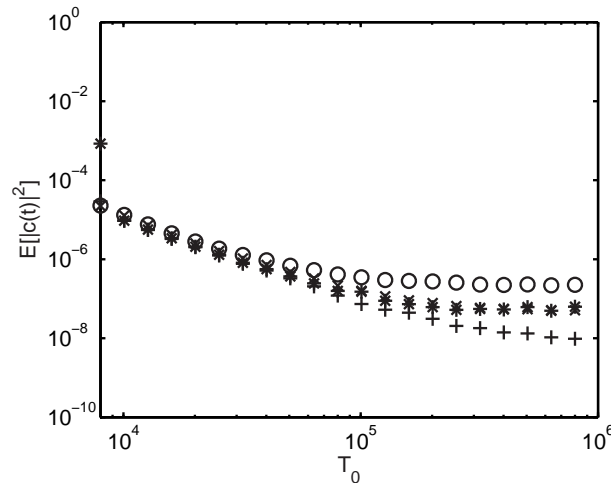
(a) Optimally tuned two-sensor algorithm.
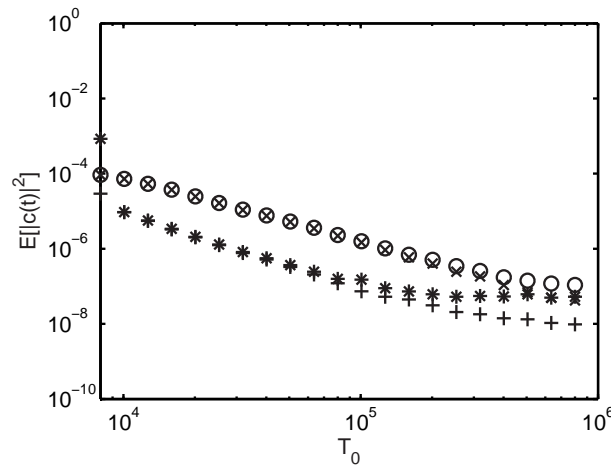
(a) Less carefully tuned two-sensor algorithm.

Figure 13. Experiment 3: Comparison of the mean-squared cancellation error, plotted versus the time-varying-frequency period T_0, yielded by hybrid SONIC (+ for SNR = 20 dB, $*$ for SNR = 10 dB) and by the two-sensor algorithm proposed by Zangi ($\times$ for SNR = 20 dB, $\circ$ for SNR = 10 dB).

5. CONCLUSIONS

The problem of suppressing nonstationary narrowband disturbances with time-varying amplitude and frequency was considered and solved using a new control architecture that combines elements of feedforward compensation and feedback control. The resulting hybrid SONIC canceller yields better performance and is more robust than the purely feedback algorithm proposed earlier. Additionally, it can be safely used in the presence of faster frequency variation.

APPENDIX Derivation of (11)

Denote by $\Delta \widehat{d}_0(t) = \widehat{d}_0(t|t-1) - d_0(t)$ and $\Delta \widehat{\omega}_0(t) = \widehat{\omega}_0(t) - \omega_0(t)$ the disturbance and frequency estimation errors, respectively. According to [16], when carrying ALF analysis, one

should neglect all terms of order higher than 1 in $\Delta\widehat{d}_0(t)$, $\Delta\widehat{\omega}_0(t)$, and $v_0(t)$, including all cross-terms.

From the first two recursions of (9), after straightforward calculations, one obtains

$$
\Delta\widehat{d}_0(t+1) = \lambda_0 e^{j\widehat{\omega}_0(t)}\Delta\widehat{d}_0(t) + \left[e^{j\widehat{\omega}_0(t)} - e^{j\omega_0(t)}\right]d_0(t)
$$
$$
+ \mu_0 e^{j\widehat{\omega}_0(t)}v_0(t). \tag{22}
$$

where $\lambda_0 = 1 - \mu_0$. Using the approximation $e^{j\Delta\widehat{\omega}_0(t)} \cong 1 + j\Delta\widehat{\omega}_0(t)$, which holds true for small frequency estimation errors, one arrives at

$$
e^{j\widehat{\omega}_0(t)} = e^{j\omega_0(t)}e^{j\Delta\widehat{\omega}_0(t)} \cong e^{j\omega_0(t)}[1 + j\Delta\widehat{\omega}_0(t)]
$$

and

$$
\left[e^{j\widehat{\omega}_0(t)} - e^{j\omega_0(t)}\right]d_0(t) \cong je^{j\omega_0(t)}\Delta\widehat{\omega}_0(t)d_0(t). \tag{23}
$$

Furthermore, under ALF rules, it holds that

$$
e^{j\widehat{\omega}_0(t)}\Delta\widehat{d}_0(t) \cong e^{j\omega_0(t)}\Delta\widehat{d}_0(t) \tag{24}
$$

and

$$
e^{j\widehat{\omega}_0(t)}v_0(t) \cong e^{j\omega_0(t)}v_0(t). \tag{25}
$$

Combining (22)–(25), one arrives at the following recursion

$$
\Delta\widehat{d}_0(t+1) \cong e^{j\omega_0(t)}[\lambda_0\Delta\widehat{d}_0(t) + j\Delta\widehat{\omega}_0(t)d_0(t) + \mu_0 v_0(t)]
$$

which, after multiplying both sides with $d_0^*(t+1) = e^{-j\omega_0(t)}d_0^*(t)$, leads to

$$
\Delta\widehat{d}_0(t+1)d_0^*(t+1) \cong \lambda_0\Delta\widehat{d}_0(t)d_0^*(t)
$$
$$
+ j\Delta\widehat{\omega}_0(t)a_0^2 + \mu_0 v_0(t)d_0^*(t). \tag{26}
$$

Let

$$
\Delta\widehat{x}(t) = \mathrm{Im}[\Delta\widehat{d}_0(t)d_0^*(t)/a_0^2], \quad e(t) = \mathrm{Im}[v_0(t)d_0^*(t)/a_0^2].
$$

Applying these shorthand definitions to (26), one obtains

$$
\Delta\widehat{x}(t+1) \cong \lambda_0\Delta\widehat{x}(t) + \Delta\widehat{\omega}(t) + \mu_0 e(t)
$$

which can also be expressed in the following polynomial form

$$
(q - \lambda_0)\Delta\widehat{x}(t) \cong \mu_0 e(t) + \widehat{\omega}_0(t) - \omega_0(t). \tag{27}
$$

Turning to the frequency update in (9), note that $\varepsilon(t) = v_0(t) - \Delta\widehat{d}_0(t)$. Using the ALF technique, one obtains

$$
\frac{\varepsilon(t)}{\widehat{d}_0(t|t-1)} \cong \frac{\varepsilon(t)}{d_0(t)} = \frac{\varepsilon(t)d_0^*(t)}{a_0^2}
$$

which leads to

$$\text{Im}\left[\frac{\varepsilon(t)}{\widehat{d}_0(t|t-1)}\right] \cong e(t) - \Delta\widehat{x}(t)$$

and

$$\widehat{\omega}_0(t+1) \cong \widehat{\omega}_0(t) + \gamma_0\mu_0[e(t) - \Delta\widehat{x}(t)].$$

The last recursion can be rewritten in the form

$$(q-1)\widehat{\omega}_0(t) \cong \gamma_0\mu_0 e(t) - \gamma_0\mu_0\Delta\widehat{x}(t). \tag{28}$$

Finally, after eliminating the term $\Delta\widehat{x}(t)$ from (27) and (28), one obtains

$$\left[1 + \frac{(\lambda_0 - q)(1-q)}{\gamma_0\mu_0}\right]\widehat{\omega}_0(t) \cong (q-1)e(t) + \omega_0(t)$$

which leads directly to (11).

REFERENCES

1. Fuller CR, Elliott SJ, Nelson PA. 1995. *Active Control of Vibration*. Academic Press.
2. Kuo SM, Morgan DR. 1996. *Active Noise Control Systems: Algorithms and DSP Implementations*. Wiley-IEEE Press.
3. Serrani A, Isidori A, Marconi L. Semiglobal nonlinear output regulation with adaptive internal model. *IEEE Transactions on Automatic Control* 2001; **46**: 1178–1194.
4. Isidori A, Marconi L, Praly L. Robust design of nonlinear internal models without adaptation. *Automatica* 2012; **48**: 2409–2419.
5. Niedźwiecki M, Meller M. A new approach to active noise and vibration control – Part I: the known frequency case. *IEEE Transactions on Signal Processing* 2009; **57**: 3373–3386.
6. Niedźwiecki M, Meller M. A new approach to active noise and vibration control – Part II: the unknown frequency case. *IEEE Transactions on Signal Processing* 2009; **57**: 3387–3398.
7. Swanson DC. Active noise attenuation using a self-tuning regulator as the adaptive control algorithm. *Proc. Internoise* 1989; **1**: 467–470.
8. Zangi KC. A new two-sensor active noise cancellation algorithm. *Proc. IEEE Int. Conf. Acoust. Speech Signal Process. (ICASSP)* 1993; **2**: 351–354.
9. Kuo SM, Morgan DR. Active noise control: a tutorial review, *Proc. IEEE* 1999; **87**: 943–973.
10. Streeter AD, Ray LR, Collier RD. Hybrid feedforward-feedback active noise control. *Proc. 2004 American Contr. Conf. (ACC)* 2004; 2876–2881.
11. Song Y, Gong Y, Kuo SM. A robust hybrid feedback active noise cancellation headset. *IEEE Transactions on Speech and Audio Processing* 2005; **13**: 607–617.
12. Lopez-Gaudana E, Betancourt P, Cruz E, Nakano-Miyatake M, Perez-Meana H. A hybrid active noise cancelling with secondary path modeling. *Proc. 2008 Midwest Symp. Circ. Syst. (MWSCAS)* 2008; 277–280.
13. Akhtar MT, Mitsuhashi W. Improving performance of hybrid active noise control systems for uncorrelated narrowband disturbances. *IEEE Transactions on Speech and Audio Processing* 2011; **19**: 2058–2066.
14. Niedźwiecki M, Meller M. Multifrequency self-optimizing narrowband interference canceller, *Proc. International Workshop on Acoustic Echo and Noise Control* 2010: 1–4.
15. Niedźwiecki M. Generalized adaptive notch smoothing revisited, *IEEE Transactions on Signal Processing* 2010; **58**: 1565–1576.
16. Tichavský P, Händel P. Two algorithms for adaptive retrieval of slowly time-varying multiple cisoids in noise, *IEEE Transactions on Signal Processing* 1995; **43**: 1116–1127.
17. Niedźwiecki M, Meller M. Self-optimizing adaptive vibration controller, *IEEE Transactions on Automatic Control* 2009; **54**: 2087–2099.
18. Niedźwiecki M, Meller M. New algorithms for adaptive notch smoothing, *IEEE Transactions on Signal Processing* 2011; **59**: 2024–2037.